



Full Length Article

Activation of Al₂O₃ surface passivation of silicon: Separating bulk and surface effectsN.E. Grant^{a,*}, S.L. Pain^a, E. Khorani^a, R. Jefferies^a, A. Wratten^a, S. McNab^b, D. Walker^c, Y. Han^c, R. Beanland^c, R.S. Bonilla^b, J.D. Murphy^a^a School of Engineering, University of Warwick, Coventry CV4 7AL, United Kingdom^b Department of Materials, University of Oxford, Oxford OX1 3PH, United Kingdom^c Department of Physics, University of Warwick, Coventry CV4 7AL, United Kingdom

ARTICLE INFO

Keywords:

ALD
Annealing
Lifetime
Silicon
Surface passivation

ABSTRACT

Understanding surface passivation arising from aluminium oxide (Al₂O₃) films is of significant relevance for silicon-based solar cells and devices that require negligible surface recombination. This study aims to understand the competing bulk and surface lifetime effects which occur during the activation of atomic layer deposited Al₂O₃. We demonstrate that maximum passivation is achieved on *n*- and *p*-type silicon with activation at ~ 450 °C, irrespective of annealing ambient. Upon stripping the Al₂O₃ films and re-passivating the surface using a superacid-based technique, we find the bulk lifetime of float-zone and Czochralski silicon wafers degrade at annealing temperatures > 450 °C. By accounting for this bulk lifetime degradation, we demonstrate that the chemical passivation component associated with Al₂O₃ remains stable at activation temperatures of 450–500 °C, achieving an SRV of < 1 cm/s on *n*- and *p*-type silicon. In conjunction with the thermal stability, we show that films in the range of 3–30 nm maintain an SRV of < 1 cm/s when annealed at 450 °C. From atomic-level energy dispersive X-ray analysis, we demonstrate that, post deposition, the interface has a structure of Si/SiO₂/Al₂O₃. After activation at > 300 °C, the interface becomes Si/Si_xAl_yO₂/Al₂O₃ due to diffusion of aluminium into the thin silicon oxide layer.

1. Introduction

Silicon photovoltaics account for > 95 % of the PV market, and this dominance is predicted to remain unchanged for the foreseeable future [1]. With the mainstream PV technology being the passivated emitter and rear cell (PERC) architecture, mitigation of surface recombination through state-of-the-art passivation layers on the front and rear of the solar cell has become ever more important. In particular, the re-emergence of aluminium oxide (Al₂O₃) in 2006 [2,3] has enabled high levels of surface passivation to be achieved on the rear side of PERC solar cells (on a *p*-type substrate), which can be attributed to the high levels of negative charge and good chemical passivation properties of the film [4]. Furthermore, with the recent introduction of passivating contact structures (e.g. TOPCon), Al₂O₃ passivation is now being utilised on the front surface of TOPCon solar cells which use *n*-type substrates [1]. As such, Al₂O₃ is playing an ever-increasing role in mitigating surface recombination on either the front or rear surface, thereby demonstrating its significance in the development of highly efficient solar cells.

There remains some uncertainty in how one can maximise the highest level of surface passivation on silicon. Often, the level of surface passivation is quantified based on the effective lifetime level achieved, which is subsequently converted into a surface recombination velocity (SRV) or surface saturation current density (*J*_{0s}) [5]. However, in doing so, the underlying bulk silicon material is assumed to be thermally stable at post-deposition annealing temperatures of < 500 °C. If this assumption is incorrect there can be substantial variability in the extracted values and thus any conclusions drawn from them. It has recently been shown that the bulk lifetime (τ_{bulk}) of float-zone (FZ) silicon is thermally unstable at temperatures between 400–800 °C, whereby τ_{bulk} has been shown to decrease by up to two orders of magnitude in some cases, independent of FZ silicon manufacturer [6,7]. High temperature (>1000 °C) thermal treatments in an oxygen ambient have been shown to annihilate the point defects responsible for this instability in the bulk lifetime, however such processes are not readily available to all research groups, and thus are often omitted in sample processing [8]. Czochralski (Cz) silicon wafers can offer greater thermal stability, as they do not

* Corresponding author.

E-mail address: nicholas.e.grant@warwick.ac.uk (N.E. Grant).<https://doi.org/10.1016/j.apsusc.2023.158786>

Received 7 July 2023; Received in revised form 16 October 2023; Accepted 28 October 2023

Available online 4 November 2023

0169-4332/© 2023 The Author(s). Published by Elsevier B.V. This is an open access article under the CC BY license (<http://creativecommons.org/licenses/by/4.0/>).

possess the same point defects created in FZ silicon, however the bulk lifetime in ‘as-received’ wafers can degrade/improve via other mechanisms, such as oxygen-related defects (thermal donors, oxygen precipitation) and metal impurities [9–12]. No silicon material can offer complete thermal stability of the bulk lifetime, and this could partly explain the variability in the passivation results reported in the literature. Setting aside material quality, and assuming similar deposition conditions, the main parameters that control Al₂O₃ surface passivation are found in the post deposition annealing conditions, as identified in Table 1. For the examples listed in Table 1, all studies have used FZ silicon as their base material without considering thermal degradation (or improvement), and each study used different post-deposition annealing conditions to achieve maximum surface passivation.

Despite variations in the bulk lifetime and post-deposition annealing conditions, the SRV values for the *n*-type samples shown in Table 1 are in relatively good agreement (e.g., 0.8–2 cm/s). In contrast the *p*-type samples show a much larger spread (e.g., 1–13 cm/s). On closer inspection, the 1 Ω-cm *p*-type data in Table 1 (i.e., last two rows) show a clear difference in the SRV when the bulk lifetime is measured (e.g., via the thickness variation method [16]). In this case, SRV was reduced from 3.2 cm/s to ~1 cm/s when accounting for variations in the bulk lifetime, however these differences could be much larger if significant bulk degradation arises.

In this work, we show how recombination at the silicon-Al₂O₃ interface can be controlled (and inhibited) in order to maximise its passivation potential for silicon based solar cells and electronic devices. We begin by examining the effective lifetime of Al₂O₃ passivated FZ and Cz silicon under varying annealing ambient and temperature. We then strip the Al₂O₃ films from selected samples and use a room temperature superacid-based surface passivation technique to accurately measure the bulk lifetime. We subject selected Al₂O₃ passivated samples to corona charging in order to separate chemical from field-effect passivation contributions as a function of annealing temperature and film thickness. We then utilise transmission electron microscopy and energy dispersive X-ray spectroscopy to analyse the composition and distribution of elements within the Al₂O₃ films as the annealing temperature is increased. Finally, we perform grazing incidence X-ray diffraction (XRD) to determine crystallisation changes in the films.

Table 1

A summary of ALD Al₂O₃ passivation on FZ silicon in key publications. All reported values are for films deposited at ~200 °C using an O₂ plasma as the co-reactant and trimethylaluminium as the precursor with the post deposition annealing (PDA) conditions as stated. Upper limit SRVs are for an injection level of 10¹⁵ cm⁻³.

Al ₂ O ₃ thickness (nm)	Resistivity (Ω-cm)	Type (<i>n/p</i>)	PDA (Temperature, ambient, time, heating source)	Upper limit SRV (cm/s)	Reference
30	3.5	<i>n</i>	450 °C/N ₂ /10 min/Furnace	0.8	[13]
30	2.2	<i>p</i>	400 °C/N ₂ /10 min/Furnace	5	[13]
30	1	<i>p</i>	425 °C/air/25 min/Hotplate	4	[14]
26	1.9	<i>n</i>	425 °C/N ₂ /30 min/RTA*	2	[2]
30	2	<i>p</i>	425 °C/N ₂ /30 min/RTA*	13	[2]
30	1	<i>n</i>	440 °C/FG**/25 min/Furnace	1.3	[15]
30	1	<i>p</i>	440 °C/FG**/25 min/Furnace	3.2	[15]
30	1	<i>p</i>	440 °C/FG**/25 min/Furnace	1 [†]	[15]

* Rapid Thermal Anneal (RTA).

** Forming Gas (FG) anneal.

[†] Measured SRV using the thickness variation method [16].

2. Experimental methods

2.1. Silicon materials

All silicon wafers used had a crystal orientation of (100). Samples studied were 5 × 5 cm unless otherwise specified. Table 2 summarises the properties of the silicon materials used in this work.

2.2. Sample processing and atomic layer deposition

Silicon samples were prepared by first immersing them in a 2 % hydrofluoric acid (HF) solution to remove any native oxide present. The samples were then immersed in a standard clean 1 (SC 1) solution consisting of H₂O, H₂O₂ (30 %) and NH₄OH (30 %) (5:1:1) at ~75 °C for 10 min. Following the SC 1 clean, the samples were once again immersed in a fresh 2 % HF solution to remove the chemical oxide formed during the cleaning process, and subsequently immersed in a 25 % TMAH etching solution at ~80 °C for 10 min. Thereafter, the samples were immersed in fresh 2 % HF solution and then immersed in a standard clean 2 (SC 2) solution consisting of H₂O, H₂O₂ (30 %) and HCl (37 %) (5:1:1) at ~75 °C for 10 min. To complete the surface pre-treatment, samples were immersed (individually) in a 2 % HF-HCl solution for ~5 s and pulled dry from the HF-HCl solution to give a hydrogen terminated surface [17]. At this point the samples were not rinsed in deionized (DI) water.

Immediately following the wet chemical cleaning process, the samples were transferred to the load lock of a Veeco Fiji G2 system which was then subsequently evacuated to mitigate any unintentional oxide formation. 5–250 cycles of Al₂O₃ (0.7–35 nm assuming a growth rate of 0.13 nm [18]) were deposited by ALD at 200 °C using an O₂ plasma source and trimethylaluminum precursor. The deposition was performed on both sides of the samples to achieve symmetrical structures. Following the Al₂O₃ depositions, the samples were annealed in a quartz tube furnace for 30 min in air at a specified annealing temperature. In some cases, silicon samples were annealed in a Surface Science Integration Solaris 100 rapid thermal processor (RTP) for 30 min at a specified annealing temperature and ambient (N₂, forming gas or N₂O). For this study, a 30 min anneal was chosen to ensure enough time was allowed to achieve maximum passivation, especially for lower annealing temperatures.

To demonstrate that thin films can yield sufficiently strong crystallisation peaks in our XRD measurements, ~10 nm (100 cycles) hafnium oxide (HfO₂) films were deposited by ALD at 200 °C using an O₂ plasma source and tetrakis(dimethylamido)hafnium precursor. Following the HfO₂ depositions, the samples were annealed in a quartz tube furnace for 30 min in air at a specified annealing temperature.

Table 2

Silicon material properties.

Growth method	Resistivity (Ω-cm)	Type (<i>n/p</i>)	Thickness (μm)	Surface finish	Figure reference
FZ*	~2	<i>n</i>	300	Mech. polished	1 (a)
Cz**	~5	<i>n</i>	130	Etched	1 (b), 2, 3 (a) 4
Cz [†]	~5	<i>p</i>	130	Etched	1 (c), 2
Cz [‡]	~2000	<i>n</i>	750	Mech. polished	5, 6

* The FZ samples were quarters cleaved from a 100 mm diameter wafer.

** The Cz samples were cleaved into ~5 × 5 cm pieces from a ~20 × 20 cm silicon wafer.

[†] The Cz wafers were gallium doped. ~5 × 5 cm pieces were cleaved from a ~13 × 13 cm silicon wafer.

[‡] The Cz samples were cleaved into ~5 × 5 cm pieces from a 12 in. silicon wafer.

2.3. Superacid passivation

Superacid passivation was performed following methods outlined in previous publications [19,20]. Firstly, the superacid solution was prepared in a nitrogen (N₂) purged glovebox to protect the chemicals from moisture. To prepare the solution, 100 mg of bis(trifluoromethane)sulfonimide (Sigma-Aldrich, 95 %) was measured out and dissolved in 50 ml of anhydrous pentane (Sigma-Aldrich, >99 %). Once prepared, the solution was stored in a glass container with an air-tight cap.

To assess the bulk lifetime of Al₂O₃ passivated samples, the Al₂O₃ films were removed in a 2 % HF solution, and then the samples were subject to the wet chemical cleaning procedure described above. Immediately following the surface pre-treatment, the silicon samples were placed in a plastic petri dish and were transferred to a glovebox. The glovebox was purged with N₂ until a relative humidity (RH) of < 25 % was achieved. The prepared superacid solution was poured into a glass beaker and then the silicon samples were immersed individually in the solution for ~ 60 s. The samples were then removed from the solution and then dried in the glovebox under N₂ ambient for ~ 30 s, after which the samples were extracted from the glovebox and measured by photoconductance decay as described below.

2.4. Characterisation

Lifetime: Photoconductance decay (PCD) effective lifetime measurements were performed at room temperature using a Sinton WCT-120 lifetime tester under transient photoconductance mode for lifetime greater than 100 μs and quasi steady-state mode for lifetimes less than 100 μs. Each result was averaged over 10 successive measurements (i.e., 10 flashes). The effective lifetime measurements are assumed to be accurate to ± 8 % [21].

Kelvin probe: KP Contact potential difference (CPD) measurements were made with a KP Technologies SKP5050 Kelvin probe with a 2 mm gold-plated tip, based on the method of Baikie et al. [22] A Fiber-Lite DC-950 Quartz Tungsten Halide lamp was used for surface photovoltage measurements.

Corona charging: Corona charging was used to determine the level of negative fixed charge in the Al₂O₃ films. The corona charge apparatus, as detailed by Bonilla et al. [23], consisted of a sharp needle held at 7 kV and positioned 7 cm from the sample. Samples were subjected to positive corona charges (e.g., H₃O⁺(H₂O)₂₋₈ [24]) for 5 s on both sides, after which they were immediately measured via transient PCD. The charge deposition rate was determined according to the Kelvin probe method of Bonilla et al., [25] which demonstrated 5 s of corona charging at 7 kV corresponded to a deposited charge Q_{corona} of $\sim 3.7 \times 10^{11}$ qcm⁻².

Transmission electron microscopy (TEM) with energy-dispersive X-ray spectroscopy (EDX). Specimens were prepared using conventional methods of grinding, polishing and ion milling to electron transparency using Ar⁺ ions at 6 kV, with a final low-energy clean at 1.5 kV to remove surface damage. They were examined in an aberration-corrected Jeol ARM200F TEM/STEM operating at 200 kV with a beam convergence angle of 22 mrad and annular dark field (ADF) detector angle of 45–180 mrad. The electron probe size was ~ 0.08 nm with a current of ~ 250 pA. EDX was performed with a windowless Oxford Instruments X-Max 100 mm² detector. The detection limit for EDX is 0.1 at% and the uncertainty in the measurement is 10 %.

XRD: Grazing incidence XRD (GI-XRD) was carried out on annealed, mirror-polished wafers coated with Al₂O₃ and HfO₂ using a 3rd generation Panalytical Empyrean XRD Diffractometer, equipped with multi-core (iCore, iCore) optics and a Pixel3D detector under Cu K_{α1/2} radiation. An incident angle of 0.5° was used for the XRD measurements. In this work HfO₂ was used as a reference sample for detecting crystallinity in thin dielectric films (~20 nm) annealed at temperatures < 600 °C.

3. Results and discussion

3.1. Activation annealing temperature & ambient

Fig. 1 (a) plots the effective lifetime (at an excess carrier density, $\Delta n = 10^{15}$ cm⁻³) of ALD Al₂O₃ coated (~20 nm) FZ 2 Ω-cm *n*-type silicon materials after annealing at temperatures between 360–520 °C in an RTP furnace for 30 min. The data in Fig. 1a show an increase in effective lifetime with annealing temperature, peaking at a temperature of 460–480 °C, and then rapidly declining with higher annealing temperatures. Notably, the annealing ambient (N₂, forming gas or N₂O) has no significant influence on the level of passivation achieved with annealing temperature implying the improvement in passivation post annealing is primarily governed by the elemental species within the film (e.g., hydrogen) rather than originating from external sources. While the optimisation study shown in Fig. 1 (a) is very important for understanding how to maximise surface passivation, interpreting the results can become difficult when considering the underlying bulk material, as this can also change with the annealing conditions used to activate the passivation. Recently it has been demonstrated that ‘as-received’ FZ silicon is thermally unstable, whereby the bulk lifetime can degrade by two orders of magnitude over the temperature region in which Al₂O₃ passivation is thermally activated due to nitrogen-vacancy defects [6,7]. Therefore, to overcome this limitation, we have assessed the bulk lifetime of the samples used in Fig. 1 (a), by stripping their Al₂O₃ coatings and subsequently re-passivating their surfaces using a room temperature superacid passivation method [19,20], as shown by the orange squares. Although the effective lifetime of the re-passivated samples is lower than that for Al₂O₃ passivation, (in keeping with the reported SRVs for Al₂O₃ and superacid of ~ 0.5 cm/s [17] and < 2 cm/s [19], respectively) the trend is still indicative of variations in the bulk lifetime. As shown by the orange squares in Fig. 1 (a), the bulk lifetime is stable up to an annealing temperature of 480 °C, above which it starts to degrade. Therefore, at annealing temperatures > 480 °C the bulk lifetime strongly influences the effective lifetime, meaning limited information regarding the stability of Al₂O₃ passivation at higher annealing temperatures can be gained from these measurements.

In an attempt to overcome the bulk lifetime limitations of FZ silicon when annealing at temperature > 480 °C, we employ photovoltaic-grade Czochralski (Cz) *n*- and *p*-type silicon wafers, the latter being doped with gallium to overcome degradation associated with the boron-oxygen defect [26], thereby enabling other bulk degradation mechanisms to be identified. Fig. 1 (b) and (c) plot the effective lifetime (at $\Delta n = 10^{15}$ cm⁻³) of ALD-grown Al₂O₃-coated (~20 nm) Cz ~ 5 Ω-cm *p*- and *n*-type silicon materials respectively after annealing in air at temperature between 300–600 °C in a quartz tube furnace for 30 min. It is clear that a peak annealing temperature of ~ 450 °C yields the highest effective lifetime on both *n*- and *p*-type silicon, as shown in Fig. 1 (b) and (c), however for higher annealing temperatures, the effective lifetime is observed to decrease, consistent with the results of Fig. 1 (a). Thus, to gain further insight on this apparent decrease in surface passivation at high annealing temperatures, we again strip their Al₂O₃ coatings and subsequently re-passivate the surfaces using room temperature superacid-based passivation. The re-passivation results presented in Fig. 1 (b) show that the bulk lifetime in *p*-type silicon is stable up to an annealing temperature of ~ 450 °C, and then decreases to the same lifetime as was achieved by the corresponding Al₂O₃ passivated samples annealed at 500 °C and 550 °C. For the bulk lifetime in *n*-type silicon, a similar trend is also observed with increasing annealing temperature, whereby the bulk lifetime steadily decreases beyond an annealing temperature of 450 °C which causes a reduction in the effective lifetime as shown in Fig. 1 (c). Therefore, as was the case for the FZ samples presented in Fig. 1 (a), the bulk lifetime of the *p*- and *n*-type samples presented in Fig. 1 (b) and (c) strongly influences the lifetime. Whilst we have been able to measure changes in the bulk lifetime, the cause for this reduction in Cz silicon is unclear. The major differences between FZ and

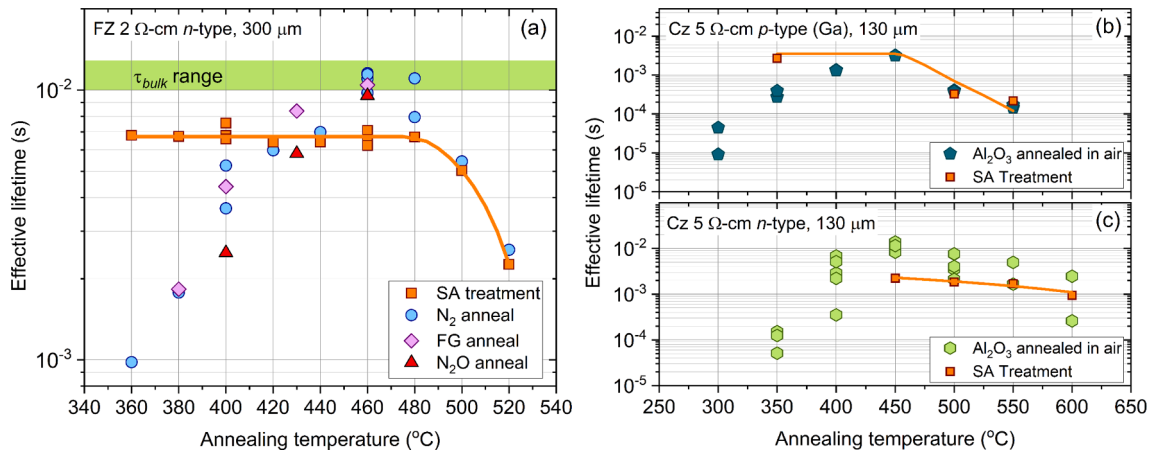


Fig. 1. (a) Effective lifetime (at $\Delta n = 10^{15} \text{ cm}^{-3}$) of ALD Al_2O_3 coated ($\sim 20 \text{ nm}$) FZ 2 $\Omega\text{-cm}$ n -type silicon samples annealed in an RTP furnace at temperatures between 360–520 °C for 30 min. The blue circles, purple diamonds and red triangles correspond to samples annealed in N_2 , FG and N_2O , respectively. (b) and (c) effective lifetime at $\Delta n = 10^{15} \text{ cm}^{-3}$ of ALD-grown Al_2O_3 -coated ($\sim 20 \text{ nm}$) Cz 5 $\Omega\text{-cm}$ p -type (gallium doped) and n -type silicon, respectively. Al_2O_3 -coated samples in (b) and (c) were annealed in air between 300 and 600 °C in quartz tube furnace for 30 min. The orange squares in all figures represent samples which had been stripped of Al_2O_3 and re-passivated by a room temperature superacid treatment. The orange lines are guides to the eye only.

Cz silicon are the oxygen and metal impurity concentrations, whereby Cz contains higher concentrations of both impurities. Grown-in metal impurities will have a detrimental effect on the bulk lifetime, however recent studies have shown that dielectric layers such as Al_2O_3 can act as gettering layers, whereby metal impurities are removed from the silicon material during annealing [27,28]. However given that we see a decline in the bulk lifetime with increasing annealing temperature suggests such a gettering mechanism is not having a significant impact on improving the bulk lifetime. In contrast, oxygen related defects are known to form recombination active thermal donors when subject to annealing temperatures between 450–650 °C, however the generation of such defects is dependent on both temperature and annealing time [29]. As such it is more likely that an oxygen related defect is causing a reduction in the bulk lifetime as shown in Fig. 1 (b) and (c). Nevertheless, whilst a degradation in the bulk lifetime is affecting our ability to quantify the impact of annealing temperature on the surface passivation quality, we can overcome this limitation by investigating the chemical and field-effect passivation of the Al_2O_3 films through alternative characterisation techniques.

3.2. Chemical and field effect passivation: Thermal stability

In order to separate the effects of chemical and field-effect passivation of the Al_2O_3 passivated samples, we subject the samples to corona discharge, whereby controlled amounts of positive charge (e.g., $\text{H}_3\text{O}^+(\text{H}_2\text{O})_{2-8}$ ions) are deposited onto the surfaces of the Al_2O_3 films [24]. The choice of positive charge is determined by the charge polarity of the film being investigated. In this case Al_2O_3 is known to possess a high level of negative charge [4], thus by depositing enough positive corona charges, we can effectively reduce the net charge to zero. This yields information on the total amount of negative charge in the Al_2O_3 film, and more importantly, an indication of the ‘interface state density – capture rate’ product ($D_{it}^* \sigma_{n/p}$) which quantifies the chemical passivation. Fig. 2 (a) and 2 (b) plot the effective lifetime (at $\Delta n = 10^{15} \text{ cm}^{-3}$) of ALD-grown Al_2O_3 -coated ($\sim 20 \text{ nm}$) Cz 5 $\Omega\text{-cm}$ n -type and p -type (gallium doped) silicon versus the amount of positive corona charge deposited on their surfaces (front and rear) respectively. In both figures, we see an initial decrease in the effective lifetime after subjecting the samples to corona charging, which can be attributed to a reduction in the net field-effect passivation of the films.

After enough positive charge has been deposited to completely offset

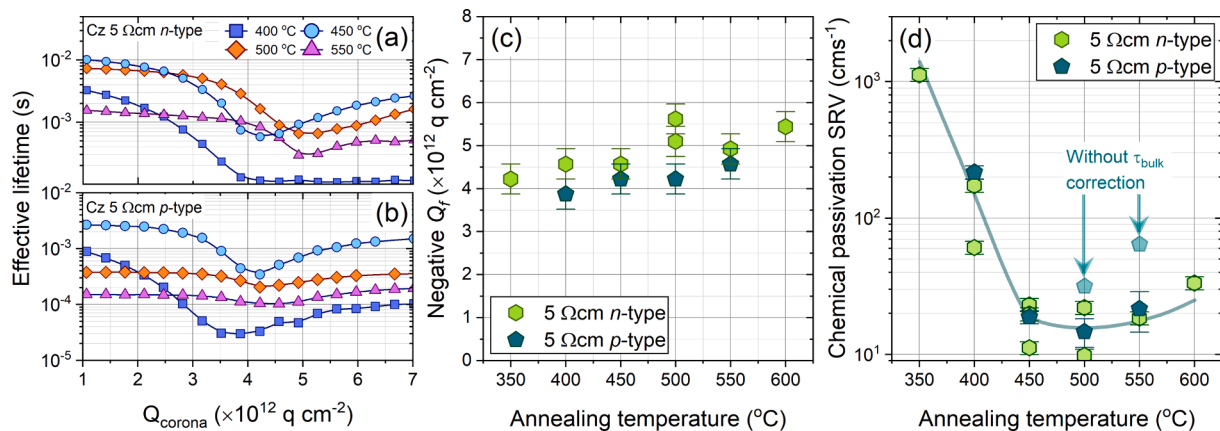


Fig. 2. (a) and (b) effective lifetime (at $\Delta n = 10^{15} \text{ cm}^{-3}$) of ALD-grown Al_2O_3 -coated ($\sim 20 \text{ nm}$) Cz 5 $\Omega\text{-cm}$ n -type and p -type (gallium doped) silicon versus the amount of positive corona charge deposited on their surfaces (front and rear) respectively. Violet squares, blue circles, orange diamonds and purple triangles correspond to samples annealed at 400 °C, 450 °C, 500 °C and 550 °C, respectively. (c) Extracted Q_f of ALD Al_2O_3 from corona charge measurements as shown in (a) and (b). (d) Chemical passivation SRV (at $\Delta n = 10^{15} \text{ cm}^{-3}$) versus annealing temperature with and without a bulk lifetime correction. Green hexagons and aqua pentagons in (c) and (d) correspond to measurements performed on Cz 5 $\Omega\text{-cm}$ n -type and p -type (gallium doped) silicon, respectively.

the negative charge within the Al₂O₃ films (e.g., net charge is < 10¹⁰ qcm⁻²), we observe a minimum in the effective lifetime measurement, which therefore provides a measurement of the chemical passivation (minimum lifetime value) and the amount of negative charge within the Al₂O₃ films prior to corona charging. Further positive corona charging beyond the minimum lifetime level increases the net charge, field-effect passivation, and thus the effective lifetime, however in this case the polarity of the net charge is positive. After ~ 7 × 10¹² qcm⁻² corona charges have been deposited onto the Al₂O₃ surfaces, no further improvement in the effective lifetime is observed implying that further charging might be leaking away due to an electrical breakdown of the dielectric layer.

From the minimum lifetime measurements presented in Fig. 2 (a) and 2 (b), we can separate the effects of chemical and field-effect passivation of the Al₂O₃ passivated samples when subject to various annealing temperatures. Fig. 2 (c) plots the amount of negative charge in the Al₂O₃ films with annealing temperature for both *n*- and *p*-type silicon samples. As should be expected, the negative charge in the Al₂O₃ films on *n*- and *p*-type silicon do not differ significantly, however their trends with annealing temperature show a slight monotonic increase in charge from -4 × 10¹² qcm⁻² at 350 °C to -5.5 × 10¹² qcm⁻² at 600 °C.

Turning our attention to the chemical passivation, Fig. 2 (d) plots the SRV corresponding to the minimum lifetime values shown in Fig. 2 (a) and 2 (b). In this case, an SRV was calculated in order to directly compare the passivation on *n*- and *p*-type samples without the influence of bulk lifetime variations using the following equation [30];

$$\frac{1}{\tau_{eff}} = \frac{1}{\tau_{bulk}} + \frac{2 \cdot S}{W}$$

where *S* corresponds to the SRV value at a specified injection level (e.g., Δ*n* = 10¹⁵ cm⁻³), *W* is the sample thickness and τ_{eff} and τ_{bulk} are the effective and bulk lifetimes, respectively, at the same specified injection level. For annealing temperatures of ≥ 500 °C the bulk lifetime measured with superacid passivation was used for calculating SRV, however for annealing temperatures < 500 °C, the silicon intrinsic lifetime limit was used to estimate the bulk lifetime [31]. For the exact calculations of SRV presented in Fig. 2 (d), the reader is referred to the data file which can be accessed via a web link at the end of this article. From Fig. 2 (d), it can be seen that the chemical passivation for Al₂O₃ on *n*- and *p*-type silicon shows a sharp decrease in SRV with annealing temperature, however upon reaching 450 °C, the chemical passivation stabilises up to a temperature of ~ 500 °C after which the SRV starts to increase. Therefore, in contrast to Fig. 1, where the lifetime immediately decreased after peaking at an annealing temperature of 450 °C, the chemical passivation remains stable up to a temperature of ~ 500 °C after which the SRV steadily increases once the limitations of the bulk lifetime are removed. For demonstration purposes, we have also included the SRV values of the Al₂O₃ passivated *p*-type samples without a bulk lifetime correction in Fig. 2 (d). This demonstrates that without careful consideration of the underlying silicon material (e.g., varying bulk lifetime), the stability of Al₂O₃ passivation can be underestimated, while the corresponding SRV can be greatly overestimated. Furthermore, by conducting our experiments on both *n*- and *p*-type silicon samples, we have demonstrated that both achieve a similar level of passivation, and both follow the same trend with annealing temperature, which could only be ascertained by separating the chemical and field-effect passivation mechanisms.

To verify the chemical passivation results presented in Fig. 2 (d), we have measured the surface photovoltage (SPV) of each sample via Kelvin probe (KP). KP measures the contact potential difference (CPD) of a sample either in the dark or under illumination, whereby the difference between these two measurements yields the SPV, e.g., SPV = CPD_{dark} - CPD_{illumination}. Measurements of SPV yield information on changes in the surface recombination occurring at the dielectric-silicon interface [32]. In this case, surface recombination refers to the interface defect density

(*D_{it}*), the electron (σ_{*n*}) and hole (σ_{*p*}) capture cross-sections, and the net fixed charge density within the film (*Q_f*) [33].

Fig. 3 (a) plots the SPV of ALD-grown Al₂O₃-coated (~20 nm) Cz 5 Ω-cm *n*-type silicon samples annealed at temperatures between 200–500 °C, and Fig. 3 (b) plots the modelled SPV response. In Fig. 3 (a), we observe two important findings (i) the SPV values are positive, which implies the charge we are measuring is negative, consistent with the results presented in Fig. 2 (c), and (ii) the trend in SPV shows a slight increase with annealing temperature indicating that as the surface passivation of the Al₂O₃ film improves with higher annealing temperatures, SPV becomes larger. To clarify the second point, we model the expected values of SPV for a theoretical Al₂O₃-Si interface, as shown in Fig. 3 (b), to demonstrate the influence of *Q_f* and *D_{it}* on the SPV response. To model the measured SPV shown in Fig. 3 (a), we employ the method described by Bonilla [32], in which we consider a 20 nm Al₂O₃ film with a dielectric permittivity of 8 deposited on a 150 μm thick, 5 Ω-cm *n*-type silicon sample (*N_{donors}* = 9 × 10¹⁴ cm⁻³). A 2 mm gold metal probe was used to measure the CPD of the sample in the KP system and is assumed to have a work function of 5.1 eV, while that for a 5 Ω-cm *n*-type silicon sample is 4.36 eV. For simplicity, we have assumed a fixed electron and hole capture cross-section of 10⁻¹⁴ cm² and 10⁻¹⁶ cm² respectively [34], but vary *Q_f* and *D_{it}* (at mid-gap) in order to demonstrate their influence on the SPV response, as shown in Fig. 3 (b). We note that the modelled SPV values are higher than those measured experimentally, thus implying the model does not fully account for all physical effects that may arise in the Al₂O₃ film or at the interface. It is known that dipole effects, hot carrier injection, and unintentional surface charges may alter the measurement. Nevertheless, we believe the trends demonstrated by the model reliably support the findings that a large part of the change in SPV with annealing temperature is due to the improving chemical passivation.

The corona charge analysis shown in Fig. 2 (b) demonstrated that these samples have *Q_f* on the order 10¹² qcm⁻². Hence, our discussion focuses on modelled SPV for *Q_f* in this region. For *Q_f* > -1 × 10¹² qcm⁻² and low values of mid-gap *D_{it}*, charge has a negligible effect on SPV, as shown by the yellow (brighter) region in the top left of Fig. 3 (b). For high surface recombination (e.g., mid-gap *D_{it}* > 10¹³ eV⁻¹cm⁻²), a higher concentration of charged carriers are stored in interface states rather than being free carriers, meaning the surface potential undergoes a smaller change under illumination due to Fermi level pinning. This results in low SPV values of 20–30 mV, as shown in Fig. 3 (a) (cf. simulated values of SPV, denoted as light green and blue shading (darker regions) in Fig. 3 (b)). In contrast, when surface recombination is suppressed (by a low *D_{it}* and/or lower minority carrier capture cross-section), a lesser proportion of the charged carriers are pinned by defect states under illumination, which results in a larger change in surface potential, leading to larger SPV values (e.g., experimental values of 100 mV, shown in Fig. 3 (a), and simulated values of ≥ 100 mV (shown in bright yellow) in Fig. 3 (b)).

Corona charge analysis demonstrated that *Q_f* does not vary substantially with annealing temperature, as shown in Fig. 2 (b), hence we conclude that the trend in SPV observed in Fig. 3 (a) results from a reduction in *D_{it}* (and hence surface recombination) as annealing temperature increases, which is consistent with the chemical passivation results presented in Fig. 2 (d). Therefore, although it is difficult to ascertain the source of passivation, the trend shown in Fig. 2 (d) is consistent with a forming gas annealed thermal SiO₂ layer whereby the additional source of passivation is hydrogen [35]. Thus, noting that plasma enhanced ALD Al₂O₃ contains ~ 3 at.% hydrogen at a deposition temperature of 200 °C, it is plausible that hydrogen is also a passivation source for Al₂O₃ on silicon [36].

3.3. Chemical and field effect passivation: Film thickness

Having established the chemical and field effect passivation of thick Al₂O₃ films post annealing between 350 and 600 °C, we now assess the

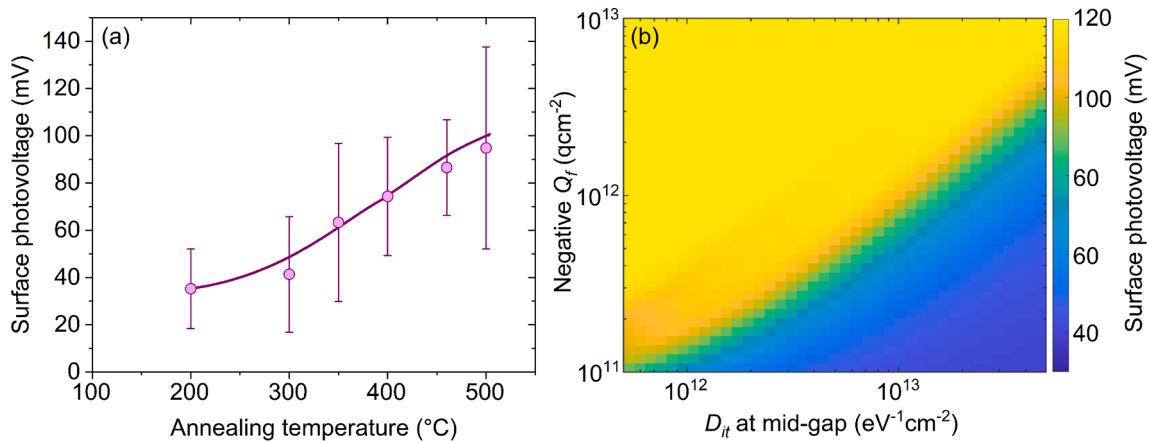


Fig. 3. Plots of the surface photovoltage (SPV) response of ALD Al₂O₃ coated (~20 nm) Cz 5 Ω-cm *n*-type silicon samples annealed at temperatures between 200–500 °C. (a) SPV as measured via Kelvin probe, and (b) modelled SPV response.

passivation mechanisms when the thickness of the Al₂O₃ film is systematically reduced from ~ 30 nm to < 1 nm. Fig. 4 (a) plots the effective lifetime (at $\Delta n = 10^{15} \text{ cm}^{-3}$) of ALD-grown Al₂O₃-coated Cz 5 Ω-cm *n*-type silicon versus ALD cycle number and the corresponding film thickness post annealing in air for 30 min at 450 °C. In contrast to previous reports in which the Al₂O₃ passivation is shown to saturate once a thickness of 10–15 nm has been achieved [4,37], Fig. 4 (a) demonstrates that maximum passivation can be achieved down to a thickness of just 25 cycles (~3 nm assuming a growth rate of 0.13 nm/cycle [18]), whereby an effective lifetime of ≥ 10 ms can be achieved, which corresponds to an upper limit SRV of 0.75 cm/s (at $\Delta n = 10^{15} \text{ cm}^{-3}$) and a surface saturation current density J_{0s} of ~ 2 fAcm⁻². However, below 25 cycles, the surface passivation rapidly decreases, whereby at 15 cycles (~2 nm) the lifetime has reduced to ~ 1 ms, which results in a 10-fold increase in the SRV and J_{0s} . For our thinnest film of just 5 cycles (~0.7 nm), the lifetime has further reduced to ~ 200 μs which corresponds to an SRV of ~ 40 cm/s and a J_{0s} of ~ 350 fAcm⁻².

To elucidate the cause of this rapid decline in passivation when the

number of ALD cycles is reduced from 25 to 5 cycles, we model the effective lifetime curves to ascertain how the chemical passivation varies with film thickness. Fig. 4 (b) shows the results of fitting the injection dependent lifetime curves of Cz 5 Ω-cm *n*-type silicon passivated with 5, 10, 15, 20 and 50 cycles of Al₂O₃. To model the lifetime curves we use a method described by Girisch *et al.* [33] and extended by Aberle *et al.* [38] which assumes the surface recombination is governed by a single defect at mid-gap [39]. We account for intrinsic recombination using the parameterisation of Niewelt *et al.* [31] and estimate the bulk lifetime through the inclusion of two mid-gap Shockley-Read-Hall (SRH) defects as validated by the injection dependent lifetime curves for the 20 and 50 cycle samples shown in Fig. 4 (b). Bulk SRH 1 is modelled using a majority carrier lifetime τ_{n0} of 63.1 ms and a minority carrier lifetime τ_{p0} of 284 μs, whilst bulk SRH 2 is modelled using a τ_{n0} of ≤ 800 μs and a τ_{p0} of 80 ms. To model the surface lifetime and more specifically the interface defect density D_{it} , we use an electron σ_n and hole σ_p capture cross-section of 10^{-14} cm^2 and 10^{-16} cm^2 respectively [34]. We use a Q_f of $-5 \times 10^{12} \text{ qcm}^{-2}$ which corresponds to the average Q_f value measured via corona

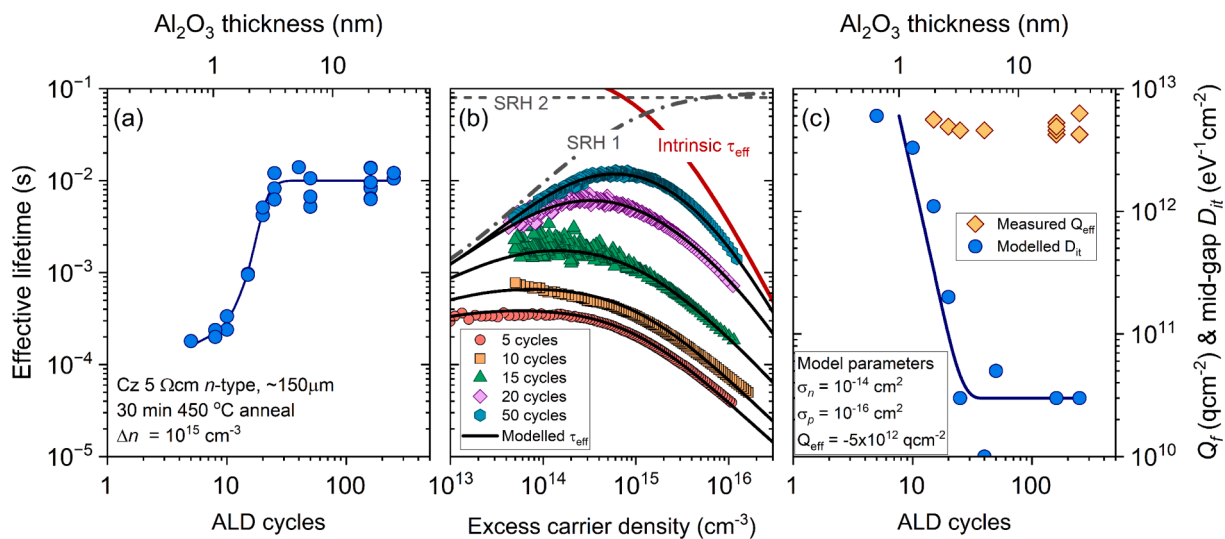


Fig. 4. (a) effective lifetime (at $\Delta n = 10^{15} \text{ cm}^{-3}$) of ALD-grown Al₂O₃-coated Cz 5 Ω-cm *n*-type silicon versus ALD cycle number and corresponding thickness post annealing in air for 30 min at 450 °C. (b) injection dependent effective lifetime curves of Al₂O₃ passivated Cz 5 Ω-cm *n*-type silicon featuring different cycles numbers and thus film thickness post annealing in air for 30 min at 450 °C. The red circles, orange squares, green triangles, purple diamonds, and turquoise hexagons correspond to 5, 10, 15, 20 and 50 ALD cycles, respectively. The solid black lines correspond to the modelled effective lifetime, the solid red line corresponds to the intrinsic lifetime limit for 5 Ω-cm *n*-type silicon [31], and the dashed/dotted grey lines correspond silicon bulk SRH lifetime limiting recombination centres. For clarity, some lifetime curves have not been plotted. (c) measured Q_f (orange diamonds), via corona charging, in the Al₂O₃ films versus ALD cycle number (i.e., thickness). The blue circles correspond to the mid-gap D_{it} from modelling of the lifetime curves shown in (b) assuming $\sigma_n = 10^{-14} \text{ cm}^2$, $\sigma_p = 10^{-16} \text{ cm}^2$ and an average $Q_f = -5 \times 10^{12} \text{ qcm}^{-2}$ as evident by the experimentally determined Q_f values (orange diamonds). In (a) and (c), the solid blue lines serve as a guide to the eye.

charging on Al₂O₃ passivated silicon comprising thicknesses in the range of 2–30 nm, as demonstrated by the orange diamonds in Fig. 4 (c). As shown in Fig. 4 (c), between a thickness of 3–30 nm (25–250 cycles) the D_{it} remains relatively constant at $\sim 3 \times 10^{10} \text{ eV}^{-1}\text{cm}^{-2}$, however when the thickness is reduced below $\sim 3 \text{ nm}$, we observe a sharp increase in the D_{it} whereby its magnitude increases by two orders of magnitude when the thickness is reduced to $\leq 1.5 \text{ nm}$. Therefore, given that Q_f is measured to be constant over a large thickness range (as shown in Fig. 4 (c)), we conclude that the sharp increase in lifetime shown in Fig. 4 (a) is predominantly characterised by a change in D_{it} . We note however that measurements of Q_f were not possible on Al₂O₃ films thinner than 2 nm, thus it is possible that substantial changes in Q_f could result when the Al₂O₃ thickness is $< 2 \text{ nm}$, meaning the D_{it} values reported for films thinner than 2 nm could be erroneous, however one would expect the D_{it} to increase as the film becomes sub-nm in thickness due to incomplete coverage, especially when approaching the lattice constant of silicon (e. g. 0.54 nm).

3.4. Interface structure and chemical composition

Until now, we have assessed the interfacial passivation properties of Al₂O₃ films annealed at various temperatures. To support our observations, we now present complementary information regarding chemical composition and elemental distribution within the Al₂O₃ films as a function of annealing temperature. Fig. 5 (a)–(f) show TEM EDX line scan measurements of Al₂O₃-coated ($\sim 20 \text{ nm}$) silicon samples annealed at temperatures between 200–500 °C for 30 min, respectively. While EDX gives only elemental composition, we can determine the silicon in oxidised form by assuming the oxide is a mix of stoichiometric Al₂O₃ and SiO₂, giving the Si(O) line in the plots. This approach is supported by the ADF-STEM images, Fig. 5 (g) and 5 (h), in which the sharp interface between crystalline silicon and the oxide is readily apparent, as is the darker band of amorphous material between the crystalline silicon and the Al₂O₃, corresponding to the lower density SiO₂ layer. Comparison of Fig. 5 (a)–(f) and (g)–(h) also reveals that the interfaces are sharper than they appear in the EDX data, i.e. some of the apparent composition gradient at the interfaces is due to spreading of the electron beam as it propagates through the specimen ($\sim 100 \text{ nm}$ in thickness). From the EDX measurements, we observe that the oxygen and total silicon (Si(E)) profiles do not change with annealing temperature, (see Fig. 5 (a) vs 5 (f)). Conversely, we do see a change in the aluminium and silicon in oxide (Si(O)) profile, particularly between annealing temperatures of 200–350 °C (Fig. 5 (a)–(c)).

To explain this transition, we first examine the data presented in Fig. 5 (a). At the Si interface, we have a silicon dioxide layer (SiO₂) and above this oxide lies an Al₂O₃ layer. The SiO₂ layer was not grown intentionally, as interfacial SiO₂ layers are known to form during the first few cycles of ALD and remain unavoidable [2,17]. After annealing at 300–350 °C, we observe that a significant amount of Al has diffused into the silicon oxide (as evidenced by a shift in the onset of the blue Al line in Fig. 5 (a)–(c)). This oxide layer remains amorphous (as evidenced in Fig. 5 (g) and (h)) with a composition of Si_xAl_yO₂, as determined from the EDX line scans in Fig. 5 (c). For annealing temperatures $> 350 \text{ °C}$ (presented in Fig. 5 (d)–(f)), elemental profiles do not vary substantially, and the interfacial oxide maintains the same composition. Therefore, although we cannot observe a compositional change for temperatures $> 350 \text{ °C}$, it is possible that very small concentrations of Al passivate dangling bonds at the Si/SiO₂ interface, thereby improving the chemical passivation, as shown in Figs. 2 and 3. In regards to the formation of field effect passivation, our EDX measurements confirm alloying/doping of the underlying SiO₂ layer by Al atoms upon thermal processing. From the literature, this is known to form electron acceptor levels within the large 9 eV bandgap of SiO₂, whereby electrons can subsequently transfer from the underlying silicon to these acceptor levels, from which a negative fixed charge is formed [40–42]. This mechanism is further supported by the results presented in Fig. 2 (a), in which the negative

charge density increases with increasing annealing temperature, which might be expected if the electrons from the silicon are thermally injected into the acceptor states of the doped SiO₂ layer.

Fig. 5 (g) and (h) show ADF-STEM images of ALD-grown Al₂O₃-coated ($\sim 20 \text{ nm}$) silicon samples annealed at temperatures of 200 °C and 500 °C for 30 min, respectively. Correspondingly, Fig. 5 (i) and (j) show cross-sectional intensity line scans from the ADF-STEM images in (g) and (h) respectively. In the as-deposited case, an oxide of $\sim 5 \text{ nm}$ thickness is present at the silicon interface, as shown in Fig. 5 (g) and inferred from (i). However upon annealing at temperatures $\geq 350 \text{ °C}$ the oxide thickness is reduced ($< 2 \text{ nm}$ in the case of a 500 °C anneal), as shown in Fig. 5 (h) and (j), with a slight compositional change due to the in-diffusion of Al, as demonstrated in Fig. 5 (c)–(f). Thus, unless ALD Al₂O₃ is annealed at temperatures $\geq 350 \text{ °C}$, the interface oxide layer remains a dynamic layer in which thickness and composition can change depending on the processing/working temperature.

3.5. Film crystallinity

The TEM images presented in Fig. 5 (e) and (f) demonstrated that, at the Si/SiO₂/Al₂O₃ interface, there was no transition in the Al₂O₃ from amorphous to crystalline on annealing at 200 °C and 500 °C. To confirm the Al₂O₃ remained amorphous further from the interface, and to ascertain whether the surface passivation characteristics of the Al₂O₃ films can be attributed to crystallinity, we performed GI-XRD measurements on polished silicon wafers coated with $\sim 20 \text{ nm}$ of Al₂O₃ that were annealed at temperatures between 200 and 450 °C for 30 min in air. Fig. 6 (a) demonstrates that at all annealing temperatures, the main feature in the XRD pattern is a set of broad peaks in the 2θ range of 50°–60° which can be attributed to the (311) plane of the underlying c-Si (100) substrate [43]. As we increase the annealing temperature, we do not observe any change in the XRD pattern. In particular, we see no peak at 68–70° (corresponding to crystalline Al₂O₃ [44]) evolving, indicating the $\sim 20 \text{ nm}$ Al₂O₃ films remain amorphous within the temperature window studied. Indeed, prior reports of ALD-grown Al₂O₃ found that annealing at $> 900 \text{ °C}$ was required for crystallization to occur [44]. To verify that this was the case with our ALD-grown films, additional GI-XRD measurements were collected on a $\sim 20 \text{ nm}$ Al₂O₃ film annealed in air at 950 °C for 30 min. The corresponding XRD pattern, which corresponds to γ -Al₂O₃, is shown in Fig. 6(a), and thus confirms our observations that Al₂O₃ does not crystallise unless annealed at very high temperatures.

To demonstrate that our GI-XRD measurement setup is suitable for identifying crystallization of ALD-grown dielectric thin films, and that the lack of observed crystallisation is not a measurement artefact, we also present equivalent XRD patterns for $\sim 20 \text{ nm}$ HfO₂ annealed over the same temperature range. A notable phase transition is observed for ALD-grown HfO₂ annealed at different temperatures, as shown in Fig. 6 (b), from amorphous to monoclinic as we have reported previously [45,46]. Additionally, X-ray reflectivity measurements made using the same system verified the presence of a $\sim 20 \text{ nm}$ Al₂O₃ film, an observation further corroborated via spectral reflectivity measurements. In contrast with the clear transition from amorphous to crystalline observed for HfO₂, no such phase transition is observed for Al₂O₃. Therefore, based on the absence of any detectable change in the Al₂O₃ films, we conclude that film crystallinity cannot explain the trends in surface passivation observed in Figs. 1 and 2.

4. Conclusion

In this work, we have conducted a thorough investigation of the mechanisms behind the activation temperature-dependent passivation quality of ALD Al₂O₃ films grown on *n*- and *p*-type silicon, separating bulk and surface recombination. We demonstrate that the ambient in which the Al₂O₃ films are annealed does not appear to have an influence on the level of passivation achieved. We also demonstrate that

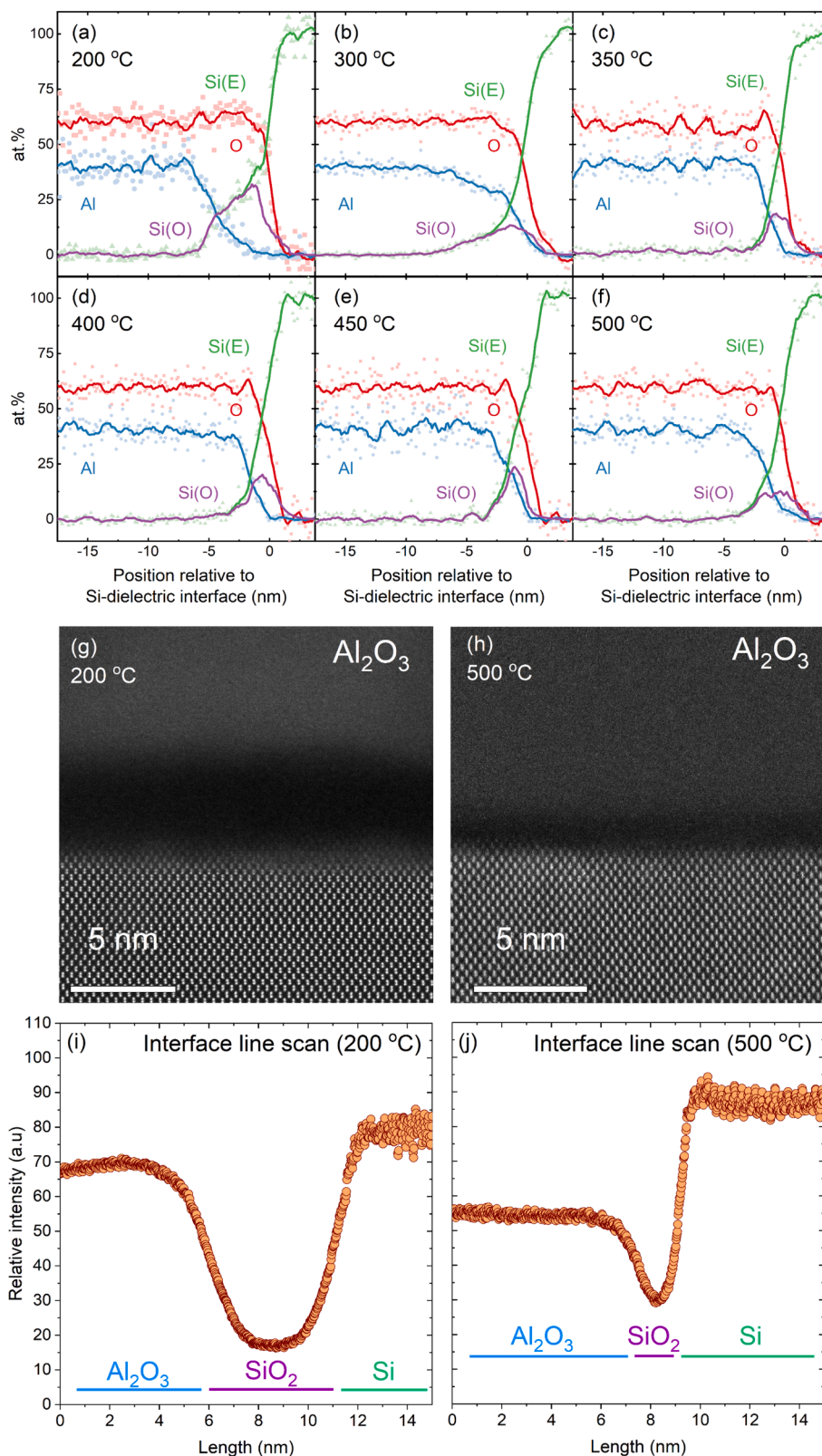


Fig. 5. (a)-(f) EDX line scan measurements of ALD Al_2O_3 coated (~ 20 nm) silicon samples annealed at temperatures between 200–500 °C for 30 min. Elements shown are displayed in atomic concentration ratios (at.%) and comprise bulk silicon (denoted Si(E), in green), silicon within the interface oxide layer (Si(O), purple), aluminium (Al, blue) and oxygen (O, red). (g) and (h) Cross-sectional ADF-STEM images of the interfacial region of ALD Al_2O_3 coated (~ 20 nm) silicon samples annealed at temperatures of 200 °C and 500 °C for 30 min, respectively. The approximate thickness of the SiO_x interfacial layer is labelled on each micrograph. (i) and (j) cross-sectional relative intensity line scans from the ADF-STEM images in (g) and (h) respectively.

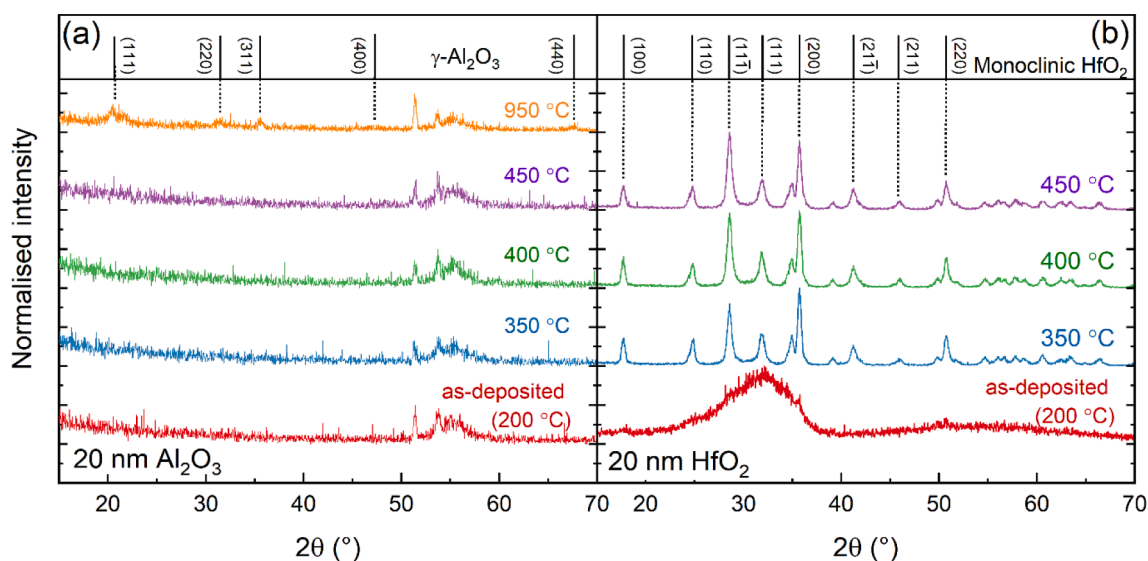


Fig. 6. GI-XRD patterns, using Cu $K_{\alpha 1/2}$, taken from polished silicon wafers coated with ~ 20 nm of (a) Al_2O_3 annealed at temperatures between 200–950 °C for 30 min in air and (b) HfO_2 annealed at temperatures between 200–450 °C for 30 min in air. The measured pattern for Al_2O_3 annealed at 950 °C corresponds to the γ - Al_2O_3 phase [43], whilst that for HfO_2 annealed at ≥ 350 °C corresponds to the monoclinic phase [44]. Patterns are vertically offset for clarity.

maximum surface passivation is achieved with a post-deposition annealing temperature of ~ 450 °C for 30 min for both n - and p -type silicon. For higher annealing temperatures, the effective lifetime was found to decrease monotonically. However, upon removing the Al_2O_3 films and re-passivating the surface using a room temperature superacid-based technique, we show that this reduction in passivation is due to degradation of the bulk lifetime. The degrading bulk lifetime dominated the overall effective lifetime, and would yield inaccurate results of the surface passivation quality if this were not understood. By accounting for the reduction in bulk lifetime, in conjunction with corona charging and Kelvin probe experiments, we were able to demonstrate that the chemical passivation of Al_2O_3 films is stable between annealing temperatures of 450–500 °C. In contrast, the negative charge within the films was found to vary with temperature, increasing from -4×10^{12} qcm^{-2} at 350 °C to -5.5×10^{12} qcm^{-2} at 600 °C. In conjunction with the thermal stability, we also examined the film thickness dependence on the chemical and field effect passivation. We found that films as thin as 3 nm can achieve maximum chemical passivation when annealed at 450 °C, achieving a D_{it} of $\sim 3 \times 10^{10}$ $\text{eV}^{-1}\text{cm}^{-2}$. Thicker films show no further reduction in the D_{it} , whilst Q_f remains constant at $\sim 5 \times 10^{12}$ qcm^{-2} within the 2–30 nm range.

We examined the chemical composition and their distribution within the Al_2O_3 films post annealing using EDX and ADF-STEM. Following annealing in air at 300–350 °C, we observe that a significant amount of Al has diffused into the silicon oxide, which remains amorphous but with a composition of $\text{Si}_x\text{Al}_y\text{O}_2$. For higher annealing temperatures e.g., >350 °C, elemental profiles do not vary substantially, and the interfacial oxide maintains the same composition, but with a reduced thickness as indicated by ADF-STEM. Despite these compositional changes at the interface, GI-XRD measurements demonstrated the Al_2O_3 films remain amorphous within the temperature range of 200–500 °C.

5. Access to data

Data underpinning figures in this paper can be freely downloaded from <https://wrap.warwick.ac.uk/180567/>. Requests for additional data should be made directly to the corresponding author.

CRediT authorship contribution statement

N.E. Grant: Conceptualization, Methodology, Validation, Formal

analysis, Investigation, Writing – original draft, Visualization, Supervision, Funding acquisition. S.L. Pain: Investigation, Formal analysis, Writing – review & editing. E. Khorani: Investigation, Formal analysis, Writing – review & editing. R. Jefferies: Investigation, Formal analysis, Writing – review & editing. A. Wratten: Investigation. S. McNab: Investigation. D. Walker: Resources, Writing – review & editing. Y. Han: Formal analysis, Investigation. R. Beanland: Formal analysis, Investigation, Resources, Writing – review & editing. R.S. Bonilla: Formal analysis, Investigation, Resources, Writing – review & editing, Supervision, Funding acquisition. J.D. Murphy: Conceptualization, Resources, Writing – review & editing, Supervision, Funding acquisition.

Declaration of Competing Interest

The authors declare the following financial interests/personal relationships which may be considered as potential competing interests: Nicholas E. Grant reports financial support was provided by Engineering and Physical Sciences Research Council. Ailish Wratten reports financial support was provided by Engineering and Physical Sciences Research Council. Sophie L. Pain reports financial support was provided by Engineering and Physical Sciences Research Council. John D. Murphy reports financial support was provided by Engineering and Physical Sciences Research Council. Edris Khorani reports financial support was provided by Engineering and Physical Sciences Research Council. Ruy S. Bonilla reports financial support was provided by Royal Academy of Engineering.

Data availability

I have provided a web link which gives access to the data presented in the paper.

Acknowledgements

S.L.P. and A.W. acknowledge funding from the Engineering and Physical Sciences Research Council Doctoral Training Partnership (EP/R513374/1). Work was supported by the EPSRC SuperSilicon PV project (EP/M024911/1), the EPSRC Charged Oxide Inversion Layer (COIL) solar cells project (EP/V037749/1 and EP/V038605/1), and the Leverhulme Trust (RPG-2020-377). R.S.B. was supported by the Royal Academy of Engineering under the Research Fellowship scheme. XRD

measurements were made using equipment housed within the X-ray Diffraction Research Technology Platform at Warwick which is supported by EPSRC (EP/V007688/1).

References

- [1] "International Technology Roadmap for Photovoltaic (ITRPV), 13th Edition " (March 2022) from <https://itrpv.dvma.org/en/>.
- [2] B. Hoex, S.B.S. Heil, E. Langereis, M.C.M. van de Sanden, W.M.M. Kessels, Ultralow surface recombination of c-Si substrates passivated by plasma-assisted atomic layer deposited Al₂O₃, *Appl. Phys. Lett.* 89 (4) (2006), 042112.
- [3] G. Agostinelli, A. Delabie, P. Vitanov, Z. Alexieva, H.F.W. Dekkers, S. De Wolf, G. Beaucarne, Very low surface recombination velocities on p-type silicon wafers passivated with a dielectric with fixed negative charge, *Sol. Energy Mater. Sol. Cells* 90 (18) (2006) 3438–3443.
- [4] G. Dingemans, W.M.M. Kessels, Status and prospects of Al₂O₃-based surface passivation schemes for silicon solar cells, *J. Vac. Sci. Technol. A* 30 (4) (2012), 040802.
- [5] K.R. McIntosh, L.E. Black, On effective surface recombination parameters, *J. Appl. Phys.* 116 (2014), 014503.
- [6] N.E. Grant, V.P. Markevich, J. Mullins, A.R. Peaker, F. Rougieux, D. Macdonald, Thermal activation and deactivation of grown-in defects limiting the lifetime of float-zone silicon, *physica status solidi (RRL) – Rapid Res. Lett.* 10 (6) (2016) 443–447.
- [7] N.E. Grant, V.P. Markevich, J. Mullins, A.R. Peaker, F. Rougieux, D. Macdonald, J. D. Murphy, Permanent Annihilation of Thermally Activated Defects Which Limit the Lifetime of Float-Zone Silicon, *Physica Status Solidi (a)* 213 (11) (2016) 2844–2849.
- [8] T. Niewelt, A. Richter, T.C. Kho, N.E. Grant, R.S. Bonilla, B. Steinhauser, J.I. Polzin, F. Feldmann, M. Hermle, J.D. Murphy, S.P. Phang, W. Kwapił, M.C. Schubert, Taking monocrystalline silicon to the ultimate lifetime limit, *Sol. Energy Mater. Sol. Cells* 185 (2018) 252–259.
- [9] J.D. Murphy, R.E. McGuire, K. Bothe, V.V. Voronkov, R.J. Falster, Minority carrier lifetime in silicon photovoltaics: The effect of oxygen precipitation, *Sol. Energy Mater. Sol. Cells* 120 (2014) 402–411.
- [10] F.E. Rougieux, N.E. Grant, D. Macdonald, Thermal deactivation of lifetime limiting grown-in point defects in n-type Czochralski silicon wafers, *Phys. Status Solidi Rapid Res. Lett.* 7 (2013) 616.
- [11] J. Haunschild, I.E. Reis, J. Geilker, S. Rein, Detecting efficiency-limiting defects in Czochralski-grown silicon wafers in solar cell production using photoluminescence imaging, *Phys. Status Solidi Rapid Res. Lett.* 5 (2011) 199.
- [12] C.A. Londos, M.J. Binns, A.R. Brown, S.A. McQuaid, R.C. Newman, Effect of oxygen concentration on the kinetics of thermal donor formation in silicon at temperatures between 350 and 500 °C, *Appl. Phys. Lett.* 62 (13) (1993) 1525–1526.
- [13] G. Dingemans, R. Seguin, P. Engelhart, M.C.M.v.d. Sanden, W.M.M. Kessels, Silicon surface passivation by ultrathin Al₂O₃ films synthesized by thermal and plasma atomic layer deposition, *physica status solidi (RRL) – Rapid Res. Lett.* 4 (1–2) (2010) 10–12.
- [14] J. Benick, A. Richter, T.-T.-A. Li, N.E. Grant, K.R. McIntosh, Y. Ren, K.J. Weber, M. Hermle, S.W. Glunz, Effect of a post-deposition anneal on Al₂O₃/Si interface properties. 35th IEEE Photovoltaic Specialists Conference, Honolulu, HI, USA, 2010.
- [15] A. Richter, S.W. Glunz, F. Werner, J. Schmidt, A. Cuevas, Improved quantitative description of Auger recombination in crystalline silicon, *Phys. Rev. B* 86 (16) (2012), 165202.
- [16] E. Yablonovitch, D.L. Allara, C.C. Chang, T. Gmitter, T.B. Bright, Unusually Low Surface-Recombination Velocity on Silicon and Germanium Surfaces, *Phys. Rev. Lett.* 57 (1986) 249.
- [17] N.E. Grant, A.I. Pointon, R. Jefferies, D. Hiller, Y. Han, R. Beanland, M. Walker, J. D. Murphy, Atomic level termination for passivation and functionalisation of silicon surfaces, *Nanoscale* 12 (33) (2020) 17332–17341.
- [18] S.L. Pain, E. Khorani, T. Niewelt, A. Wratten, G.J. Paez Fajardo, B.P. Winfield, R. S. Bonilla, M. Walker, L.F.J. Piper, N.E. Grant, J.D. Murphy, "Electronic Characteristics of Ultra-Thin Passivation Layers for Silicon Photovoltaics," *Advanced Materials, Interfaces* 9 (28) (2022) 2201339.
- [19] N.E. Grant, T. Niewelt, N.R. Wilson, E. Wheeler-Jones, J. Bullock, M. Al-Amin, M. C. Schubert, A.C. van Veen, A. Javey, J.D. Murphy, Superacid-Treated Silicon Surfaces: Extending the Limit of Carrier Lifetime for Photovoltaic Applications, *IEEE J. Photovoltaics* 7 (2017) 1574–1583.
- [20] A.I. Pointon, N.E. Grant, E.C. Wheeler-Jones, P.P. Altermatt, J.D. Murphy, Superacid-derived surface passivation for measurement of ultra-long lifetimes in silicon photovoltaic materials, *Sol. Energy Mater. Sol. Cells* 183 (2018) 164–172.
- [21] A.L. Blum, J.S. Swirhun, R.A. Sinton, F. Yan, S. Herasimenka, T. Roth, K. Lauer, J. Haunschild, B. Lim, K. Bothe, Z. Hameiri, B. Seipel, R. Xiong, M. Dhamrin, J. D. Murphy, Inter-laboratory study of eddy-current measurement of excess-carrier recombination lifetime, *IEEE J. Photovoltaics* 4 (2014) 525–531.
- [22] I.D. Baikie, S. Mackenzie, P.J.Z. Estrup, J.A. Meyer, Noise and the Kelvin method, *Rev. Sci. Instrum.* 62 (5) (1991) 1326–1332.
- [23] R.S. Bonilla, C. Reichel, M. Hermle, P. Hamer, P.R. Wilshaw, Long term stability of c-Si surface passivation using corona charged SiO₂, *Appl. Surf. Sci.* 412 (2017) 657–667.
- [24] J.D. Skalny, J. Orszagh, S. Matejčík, N.J. Mason, J.A. Rees, Y. Aranda-Gonzalvo, T. D. Whitmore, A mass spectrometric study of ions extracted from point to plane DC corona discharge fed by carbon dioxide at atmospheric pressure, *Int. J. Mass Spectrom.* 277 (1) (2008) 210–214.
- [25] R.S. Bonilla, N. Jennison, D. Clayton-Warwick, K.A. Collett, L. Rands, P. R. Wilshaw, Corona Charge in SiO₂: Kinetics and Surface Passivation for High Efficiency Silicon Solar Cells, *Energy Procedia* 92 (2016) 326–335.
- [26] T. Niewelt, J. Schön, W. Warta, S.W. Glunz, M.C. Schubert, Degradation of Crystalline Silicon Due to Boron-Oxygen Defects, *IEEE J. Photovoltaics* 7 (1) (2017) 383–398.
- [27] A. Liu, S.P. Phang, D. Macdonald, Gettering in silicon photovoltaics: A review, *Sol. Energy Mater. Sol. Cells* 234 (2022), 111447.
- [28] A.Y. Liu and D. Macdonald, Impurity gettering effect of atomic layer deposited aluminium oxide films on silicon wafers, *Appl. Phys. Lett.*, vol. 110, no. 19, 2017.
- [29] R. Basnet, H. Sio, M. Siriwardhana, F.E. Rougieux, D. Macdonald, Ring-like Defect Formation in N-Type Czochralski-Grown Silicon Wafers during Thermal Donor Formation, *Physica Status Solidi (a)* 218 (4) (2021) 2000587.
- [30] A.B. Sproul, Dimensionless solution of the equation describing the effect of surface recombination on carrier decay in semiconductors, *J. Appl. Phys.* 76 (5) (1994) 2851–2854.
- [31] T. Niewelt, B. Steinhauser, A. Richter, B. Veith-Wolf, A. Fell, B. Hammann, N. E. Grant, L. Black, J. Tan, A. Youssef, J.D. Murphy, J. Schmidt, M.C. Schubert, S. W. Glunz, Reassessment of the intrinsic bulk recombination in crystalline silicon, *Sol. Energy Mater. Sol. Cells* 235 (2022), 111467.
- [32] R.S. Bonilla, Modelling of Kelvin probe surface voltage and photovoltage in dielectric-semiconductor interfaces, *Mater. Res. Express* 9 (8) (2022), 085901.
- [33] R.B.M. Girisch, R.P. Mertens, R.F.D. Keersmaecker, Determination of Si-SiO₂ recombination parameters using a gate-controlled point-junction diode under illumination, *IEEE Trans. Electron Devices* 35 (2) (1988) 203–222.
- [34] L.E. Black, *New Perspectives on Surface Passivation: Understanding the Si-Al₂O₃ Interface*, 1 ed., (Springer Theses). Springer Cham, 2016.
- [35] E.H. Nicollian, J.R. Brews, *MOS (Metal Oxide Semiconductor) Physics and Technology*, John Wiley and Sons, New York, 1982, p. 784.
- [36] G. Dingemans, F. Einsele, W. Beyer, M.C.M. van de Sanden, W.M.M. Kessels, Influence of annealing and Al₂O₃ properties on the hydrogen-induced passivation of the Si/SiO₂ interface, *J. Appl. Phys.* 111 (9) (2012) pp.
- [37] J. Schmidt, B. Veith, F. Werner, D. Zielke, and R. Brendel, Silicon surface passivation by ultrathin Al₂O₃ films and Al₂O₃/SiN_x stacks, in: 2010 35th IEEE Photovoltaic Specialists Conference, 20–25 June 2010 2010, pp. 000885–000890, <http://doi.org/10.1109/PVSC.2010.5614132>.
- [38] A.G. Aberle, S. Glunz, W. Warta, Impact of illumination level and oxide parameters on Shockley–Read–Hall recombination at the Si-SiO₂ interface, *J. Appl. Phys.* 71 (9) (1992) 4422–4431.
- [39] Calculator map on PV Lighthouse. <http://www.pvlighthouse.com.au> (accessed).
- [40] D. König, D. Hiller, S. Gutsch, M. Zacharias, S. Smith, Modulation Doping of Silicon using Aluminium-induced Acceptor States in Silicon Dioxide, *Sci. Rep.* 7 (1) (2017) 46703.
- [41] J.-P. Lehtö, Z.J. Rad, S. Granroth, M. Yasir, M. Punkkinen, R. Punkkinen, H.-P. Hedman, J.-P. Rueff, I.T.S. Rauha, H. Savin, P. Laukkanen, K. Kokko, Observation of Si 2p Core-Level Shift in Si/High-κ Dielectric Interfaces Containing a Negative Charge, *Adv. Electron. Mater.* 7 (4) (2021) 2100034.
- [42] O.A. Dicks, J. Cottom, A.L. Shluger, V.V. Afanas'ev, The origin of negative charging in amorphous Al₂O₃ films: the role of native defects, *Nanotechnology* 30 (20) (2019), 205201.
- [43] R.-S. Zhou, R.L. Snyder, Structures and transformation mechanisms of the η, γ and θ transition aluminas, *Acta Crystallogr. B* 47 (5) (1991) 617–630.
- [44] C.E. Curtis, L.M. Doney, J.R. Johnson, Some Properties of Hafnium Oxide, Hafnium Silicate, Calcium Hafnate, and Hafnium Carbide, *J. Am. Ceram. Soc.* 37 (10) (1954) 458–465.
- [45] A. Wratten, S.L. Pain, D. Walker, A.B. Renz, E. Khorani, T. Niewelt, N.E. Grant, J. D. Murphy, Mechanisms of Silicon Surface Passivation by Negatively Charged Hafnium Oxide Thin Films, *IEEE J. Photovolt.* 13 (1) (2023) 40–47.
- [46] A. Wratten, D. Walker, E. Khorani, B.F.M. Healy, N.E. Grant, J.D. Murphy, Hafnium oxide: A thin film dielectric with controllable etch resistance for semiconductor device fabrication, *AIP Adv.* 13 (2023), 065113.